Journal of Engg. Research ICAPIE Special Issue pp. 19-26 DOI:10.36909/jer.ICAPIE.15039

Behavior of 316L Stainless Steel Under Static and Dynamic Loading Conditions

Chandra Shekhar Kumar* and Girija Shankar Mahobia

Department of Metallurgical Engineering, Indian Institute of Technology (BHU), Varanasi
**Corresponding Author: chandrask.rs.met16@iitbhu.ac.in*

ABSTRACT

In the present study, 316L stainless steel was characterized for microstructure and mechanical behavior under static and dynamic loading conditions. It showed a high ratio of tensile strength to yield strength with good ductility. Experiments on strain controlled tests, performed at 0.25 Hz frequency, resulted in reduction of fatigue life with increasing total strain amplitude. At higher strain amplitudes, secondary cyclic hardening was noticed. In contrast, cyclic hardening was observed for initial few cycles followed by softening up to failure at lower strain amplitudes.

Keywords: 316L Stainless steel; Tensile properties; Strain controlled tests.

INTRODUCTION

Metallic materials are used in variety of an orthopedic implant material. Stainless steels, titanium and its derivatives and Co-Cr alloys have long been utilized in biomedical applications for fracture fixation and joint replacement. Among these metals, SS 316L has low cost, good corrosion resistance and acceptable biocompatibility (Jinlong, Tongxiang, and Chen 2016; Nishiguchi et al. 2001). It is used for manufacturing implants such as artificial joint, bone plate and stent. Austenitic, ferritic and martensitic are the three grades of stainless steels. Austenitic grade of stainless steels are non-magnetic. SS 316L contains a high amount of nickel (10-12 wt%), stabilizing the austenite structure and makes it non-magnetic. In addition, SS 316L has a large amount of chromium and a small amount of molybdenum to develop resistance for corrosion in simulated body fluids (Hank's and Eagle's minimum essential medium (MEM)) (Tang et al. 2006). A very complicated procedure is followed to place the implants in the human body and it may cause local inflammation, which may affect the corrosion resistance (Brooks, Brooks, and Ehrensberger 2017). Pitting is the most severe damaging phenomenon of stainless steels. The pits formed due to corrosion may act as crack initiation sites during cyclic loading. Implant devices such as bone plates and artificial hip joints made up of SS 316L gets fractured in the human body due to the combined effect of corrosion and fatigue (Sivakumar, Kamachi Mudali, and Rajeswari 1995).

SS 316L is popular structural steel and used in power plants' applications where it undergoes dynamic loading conditions at room temperature (RT). Therefore, the fatigue life of SS 316L is an important design criterion for such components. Alain et al. investigated the LCF behavior of SS 316L with constant plastic strain control mode at 2 x 10-3 s-1 constant rate of plastic strain, with temperatures varying between 20 °C - 600 °C (Alain, Violan, and Mendez 1997). Hong et al. investigated the influence of temperature on LCF properties of SS 316L at 10-3 constant rate of strain and studied the effect of strain rate on LCF behavior (Hong, Lee, and Byun 2007; Hong, Yoon, and Lee 2003).

The present investigation discusses the mechanical behavior of SS 316L, which includes microstructural characterization, phase analysis, tensile and LCF properties. LCF experiments were performed at RT with 0.25 Hz constant frequency, for different total strain amplitudes. The cyclic stress response, strain-life and strain energy density-life behavior were investigated.

EXPERIMENTAL PROCEDURE

SS 316L plates of size 300 mm x 300 mm x18 mm in the solution annealed condition was provided by M/s Jindal Stainless Ltd. (JSL)-Hisar. Table 1 corresponds to the chemical composition of this alloy. Sample of SS 316L was polished by various grades of emery papers, followed by alumina powder suspension using velvet cloth. It was cleaned in water, etched with aqua regia, and microstructure observed by an optical microscope. X-ray technique (XRD)

Table 1. Chemical composition of the SS 316L (wt %).

C	Cr	Mn	Ni	Si	Mo	N (PPM)	Cu	S	P	Fe
0.024	16.3	1.2	10	0.25	2	343	0.4	0.002	0.04	Balance

having source as Cu-Kα was used for the phase analysis. ASTM A 370 tensile test samples were prepared (gauge diameter: 25 mm & gauge length: 6.25 mm). An extensometer was mounted to record the induced strain at 5× 10-4 strain rate. Cylindrical fatigue samples were machined, as reported by Kumar et al. (Kumar et al. 2020). The samples' gauge section was polished on emery papers of different grit sizes and lastly by alumina suspension. LCF tests of 316L were conducted at various total strain amplitudes (Δεt/2) ranging from ± 0.30% - ± 1.0%, at 0.25 Hz constant frequency, under fully reversed loading. The details of equipment used was given elsewhere (Kumar et al. 2020). The strain was controlled by using an extensometer (Model: MTS 632.53F). The total, plastic, and elastic strain with associated stress were recorded by controller software (Flex test 40) during testing.

RESULTS AND DISCUSSION

Microstructural characterization

The optical micrograph of SS 316L with equiaxed austenite grains having a mean intercept length of 29±4 μm is shown in Figure 1a. A small number of annealing twins were also visualized within the grains. Figure 1b shows

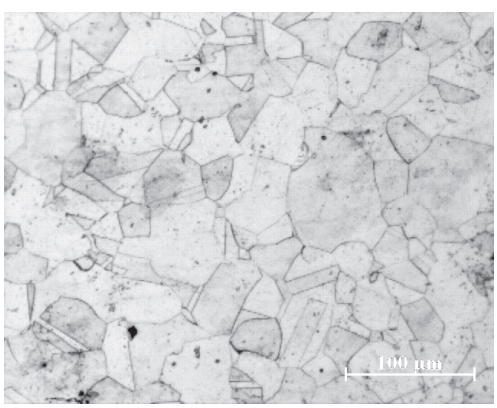

(a)

Figure 1. Optical micrograph (a) and

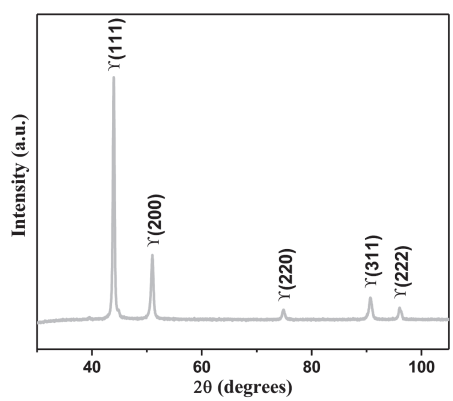

(b)

Figure 1.(b) of SS 316L.

X-Ray diffractogram

the X-ray diffractogram of SS 316L. It may be seen that there are austenite peaks. The 316L SS's hardness was recorded using a vickers hardness tester at 5 kg load and was found to be 140±6 HV.

Tensile properties

The different parameters including elongation to fracture, ultimate tensile strength (UTS) and yield strength (YS) were recorded after tensile testing of SS 316L at RT. The engineering stress-strain curve is revealed in Figure 2a and various tensile properties are recorded and shown in Table 2.

Table 2. Tensile properties of SS 316L.

YS	UTS	Uniform strain (%)	Total strain (%)	UTS/YS
279	616	58	74	2.21

The ratio UTS/YS is more than 2, which shows the significant work hardening behavior of SS 316L. The strain before the onset of necking is called as uniform strain, which is a significant parameter for the cold working of any material and was found to be 58%.

True stress-true strain curve was plotted from the engineering stress-strain plot using the following relations (Dieter 1988).

$$\sigma = S(1+e) \quad (1)$$

$$\varepsilon = \ln(1+e) \quad (2)$$

Where e, S, ε and σ are engineering strain, engineering stress, true strain and true stress, respectively. These relationships are valid only up to UTS as necking starts after UTS.

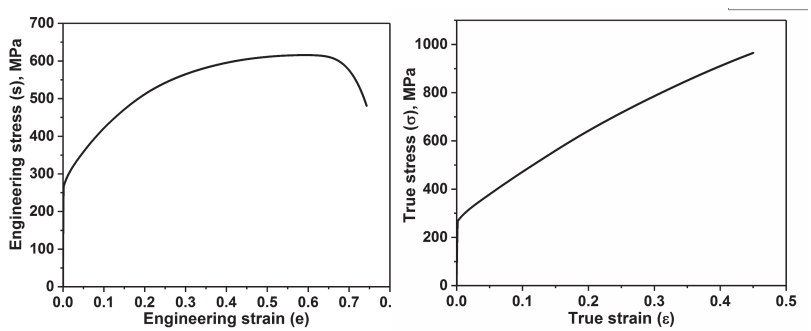

(a) (b)

Figure 2. Stress-strain curves of the SS 316L: engineering stress-strain curve (a) **Figure 2.** true stress-true strain curve (b)

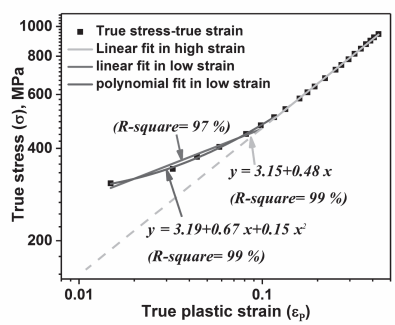

(c)

Figure 2. log-log plot of true stress-true plastic strain (c).

True stress- true strain plot is shown in Figure 2b, which reveals the significant work hardening. Figure 2c shows the plot of true stress vs true plastic strain. There was a difference in the slope of the curve at higher and lower strains. A linear relationship was observed at higher strains, whereas it deviated from linearity at lower strains. An attempt was made to fit this curve at lower strains. Continuous change in the slope of the curve was observed and a second-degree polynomial was fitted. The equation of the fitted line and curve at higher and lower strains was found as given in Figure 2c.

The difference in slope of the log-log curve of the true stress-true plastic strain may be due to the change in deformation mechanisms at higher and lower strain. It has been well documented for low stacking fault energy materials that many microstructural features appear with increase in stress level during monotonic static loading (Kundu and Chakraborti 2010; Li et al. 2013). At the very low stresses, single slip is there and dislocation density increases with increase in strain. More slip system activates with increase in stress. Also, twinning and martensitic transformation takes place depending on the stress level (Shen et al. 2012).

Low cycle fatigue behavior

LCF tests at RT were performed at different $\Delta\varepsilon t/2$ varying from ± 0.3% - ± 1.0%, at 0.25 Hz constant frequency, to examine the LCF behavior. A very distinct cyclic stress response revealed in Figure 3a, was seen. There was primary cyclic hardening for the initial few cycles at all the $\Delta\varepsilon t/2$. At lower $\Delta\varepsilon t/2$ i.e.± 0.3% and ± 0.4%, primary cyclic hardening was observed for the first 30 cycles and thereafter cyclic softening up to failure was recorded. This type of LCF behavior was observed by Ho et al. (Ho et al. 2020). At the intermediate $\Delta\varepsilon t/2$ of ± 0.5% and ± 0.6%, primary cyclic hardening for the first 30 cycles was recorded and then cyclic softening for most fatigue life and a mild secondary hardening was seen. There was primary cyclic hardening for the initial 20 cycles at $\Delta\varepsilon_t/2$ of ± 0.8%. After that,

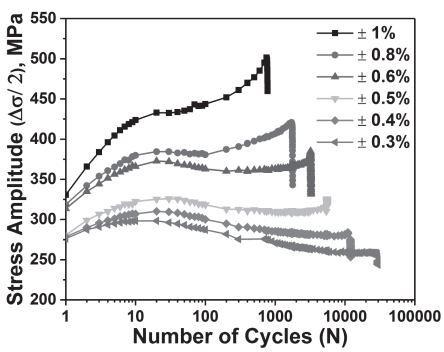

(a)

Figure 3. Cyclic stress response of SS 316L tested at 0.25 Hz frequency (a)

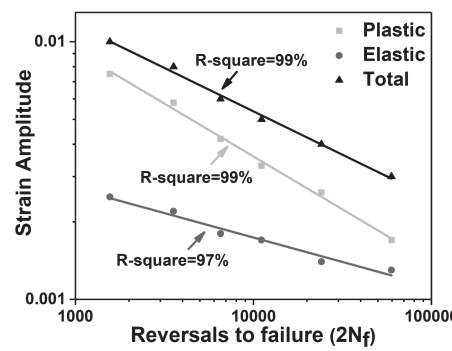

(b)

Figure 3.double logarithmic plot of strain amplitudes vs reversals to failure (2Nf) (b)

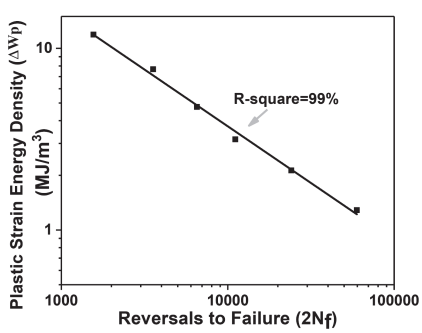

(c)

Figure 3.the dependence of reversals to failure on plastic strain energy density of SS 316L (c).

cyclic softening (till 100 cycles) followed by a prominent secondary cyclic hardening was seen. Primary cyclic hardening was seen during the first 20 cycles, thereafter stabilization (40 cycles) was observed and after that, secondary cyclic hardening was seen at the $\Delta\varepsilon_t/2$ of ± 1.0%.

Prominent secondary cyclic hardening was recorded with increased strain amplitude. Hong et al. (Hong, Lee, and Byun 2007) observed similar stress response of SS 316L at RT which were tested at 1 x 10^{-3} s^{-1} constant strain rate. In contrast, continuous softening after initial hardening was observed at all the ranges of strain amplitudes (Hong, Yoon, and Lee 2003). Lei et al. (Lei et al. 2019) observed similar stress response for coarse grained 316L when tested for LCF at 3.6 x 10-2 s-1 constant strain rate. There is increase in dislocation density with cyclic loading for the initial few cycles, which causes the primary cyclic hardening. Rearrangement of dislocation and formation of dislocation walls due to secondary slip activation with the enhancing number of cycles causes cyclic softening (Pham et al. 2013) . There is deformation-induced martensitic transformation in metastable stainless steels with low stacking fault energy which strongly depends on strain and strain rate (Shen et al. 2012). In this investigation, all the LCF tests were conducted at 0.25 Hz constant frequency. Strain rate, strain amplitude and frequency of the cyclic loading in fully reversed conditions can be related as shown in Equation 3. Strain rate becomes equal to strain amplitude at 0.25 Hz frequency and there is an

Strain rate = 4 × strain amplitude × frequency (3)

increase in strain rate with increased strain amplitude. The no. of cycles corresponding to maximum primary hardening decreases with increase in $\Delta\varepsilon_t/2$ which is due to increased dislocation activity with strain rate (Lu and Lu 2004). The primary cyclic hardening is related to the enhanced dislocation density, whereas secondary hardening may be due to the martensitic transformation induced by deformation (Jeon et al. 2008).

The LCF test results of SS 316L tested at 0.25 Hz constant frequency are tabulated in Table 3. The various fatigue parameters like σ·f, b, ε·f and c were obtained with the help of Figure 3b based on the relationship shown in Equation 4 (Guguloth et al. 201 4).

Table 3. LCF test results of SS 316L tested at constant frequency of 0.25 Hz at half-life cycle.

Total strain amplitude ($\Delta\varepsilon_t/2$), %	Plastic strain amplitude ($\Delta\varepsilon_p/2$), %	Elastic strain amplitude ($\Delta\varepsilon_e/2$), %	Number of cycles to failure (N_f)
0.3	0.17	0.13	29820
0.4	0.26	0.14	12049
0.5	0.33	0.17	5551
0.6	0.42	0.18	3268
0.8	0.58	0.22	1779
1.0	0.75	0.25	781

$$\frac{\Delta\varepsilon_t}{2} = \frac{\Delta\varepsilon_e}{2} + \frac{\Delta\varepsilon_p}{2} = \frac{\sigma'_f}{E}(2N_f)^b + \varepsilon'_f(2N_f)^c \quad (4)$$

In Equation 4,$\Delta\varepsilon_t/2$, $\Delta\varepsilon_e/2$, $\Delta\varepsilon_p/2$, ε_f, c, $\sigma\varepsilon_f$, b, E and N_f are total strain amplitude, elastic strain amplitude, plastic strain amplitude, fatigue ductility coefficient, fatigue ductility exponent, fatigue strength coefficient, fatigue strength exponent, modulus of elasticity and fatigue life, respectively.

Figure 3c shows the plot of plastic strain energy density vs. $2N_f$. Fatigue life was also analyzed according to the relationship established in Equation 5 (Praveen and Singh 2008; Song et al. 2011).

$$\Delta W_p = W'_f (2N_f)^{\beta} \quad (5)$$

In Equation 5, ΔW_p, W'_f and β are plastic strain energy density, plastic strain energy coefficient and plastic strain energy density exponent, respectively. Hysteresis loop area is the plastic strain energy density, at half-life cycle (Verma et al. 2016). Various parameters σf, b, ε'_f, c, Wf and β are determined by least-square linear fitting of these plots and their values are listed in Table 4. The plastic strain and plastic strain energy play a decisive part in the cyclic damage of the materials. The fatigue life and plastic strain energy density relation provides a measure of fatigue damage.

Table 4. Various fatigue parameters estimated from the plastic strain energy density-life and strain-life relationship.

σ'_f (MPa)	b	ε'_f	c	W'_f	β	b+c
1995	-0.19	0.16	-0.41	1169	-0.62	-0.60

A correlation between plastic strain energy density exponent (β), fatigue ductility exponent and fatigue strength exponent is established for 9Cr-1Mo steel at room temperature, as shown in Equation 6 (Verma et al. 2016). This relation is also established for this steel as the value of β and b+c are found comparable (Table 4).

$$\beta = b + c \quad (6)$$

Figure 4 reveals the fracture behavior of LCF tested specimens at ±0.4% and ±1.0% strain amplitudes. Figures 4a and 4c are showing the overall fracture region of samples tested at ±0.4% and ±1.0%, respectively, whereas Figures 4b and 4d are showing the corresponding fatigue striations at higher magnification.

Inter-spacing between the fatigue striations at total strain amplitude ±1.0% is larger than that of the ±0.4%. These striations are related to crack propagation. Larger inter-striation spacing signifies the higher crack propagation rate.

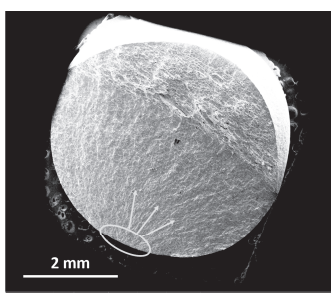

(a)

Figure 4. Fractographs of SS 316L samples tested at $\Delta\varepsilon_t/2$ of: ± 0.4% (a, b) and ± 1.0% (c, d). Encircled regions andarrows show the crack initiation site and direction of crack propagation, respectively.

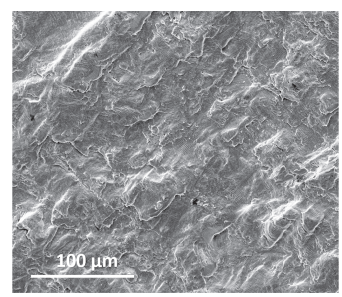

(b)

Figure 4. Fractographs of SS 316L samples tested at $\Delta\varepsilon_t/2$ of: ± 0.4% (a, b) and ± 1.0% (c, d). Encircled regions andarrows show the crack initiation site and direction of crack propagation, respectively.

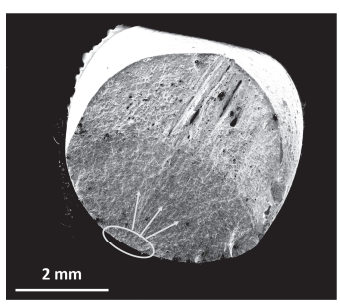

(c)

Figure 4. Fractographs of SS 316L samples tested at $\Delta\varepsilon_t/2$ of: ± 0.4% (a, b) and ± 1.0% (c, d). Encircled regions andarrows show the crack initiation site and direction of crack propagation, respectively.

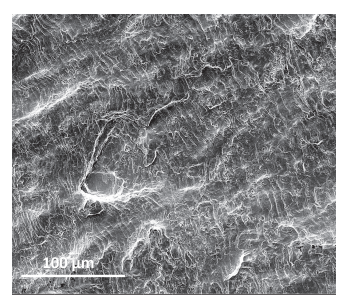

(d)

Figure 4. Fractographs of SS 316L samples tested at $\Delta\varepsilon_t/2$ of: ± 0.4% (a, b) and ± 1.0% (c, d). Encircled regions andarrows show the crack initiation site and direction of crack propagation, respectively.

CONCLUSION

From the present work -Behavior of 316L stainless steel under static and dynamic loading conditions, it has been concluded that SS 316L shows fully austenitic microstructure in solution annealed condition with hardness of 140 ± 6 Hv. Yield strength, tensile strength and total strain was recorded as 279 MPa, 616 MPa and 74 %, respectively. The high ratio of UTS/YS= 2.21 shows that this steel is highly work hardenable. Moreover, there was decrease in cyclic life with enhancing $\Delta\varepsilon t/2$ from ± 0.3 % - ± 1.0%. The plastic strain and strain energy play a key role in fatigue failure of the SS 316L. Fractographs showed the drastic reduction in cyclic life at higher $\Delta\varepsilon t/2$ was associated with rapid crack propagation. Also, at the higher strain amplitudes (≥ ± 0.6 %), prominent secondary hardening was observed due to the high strain rate and martensitic transformation induced by deformation. The number of cycles corresponding to attainment of maximum primary cyclic hardening was found to reduce with increasing strain amplitude due to increased strain rate.

REFERENCES

Alain, R., P. Violan, and J. Mendez. 1997. "Low Cycle Fatigue Behavior in Vacuum of a 316L Type Austenitic Stainless Steel between 20 and 600°C Part I: Fatigue Resistance and Cyclic Behavior." Materials Science and Engineering A 229(1–2): 87–94.

Brooks, Emily K., Richard P. Brooks, and Mark T. Ehrensberger. 2017. "Effects of Simulated Inflammation on the Corrosion of 316L Stainless Steel." Materials Science and Engineering C 71: 200–205.

"Dieter G. E. 1988. "Mechanical Metallurgy", Mcgraw-Hill book company, Singapore: 283-285.

Guguloth, Krishna, S. Sivaprasad, D. Chakrabarti, and S. Tarafder. 2014. "Low-Cyclic Fatigue Behavior of Modified 9Cr-1Mo Steel at Elevated Temperature." Materials Science and Engineering A 604: 196–206.

Ho, H. S. et al. 2020. "Low-Cycle Fatigue Behavior of Austenitic Stainless Steels with Gradient Structured Surface Layer." International Journal of Fatigue 134(October 2019).

Hong, Seong Gu, Soon Bok Lee, and Thak Sang Byun. 2007. "Temperature Effect on the Low-Cycle Fatigue Behavior of Type 316L Stainless Steel: Cyclic Non-Stabilization and an Invariable Fatigue Parameter." Materials Science and Engineering A 457(1–2): 139–47.

Hong, Seong Gu, Samson Yoon, and Soon Bok Lee. 2003. "The Effect of Temperature on Low-Cycle Fatigue Behavior of Prior Cold Worked 316L Stainless Steel." International Journal of Fatigue 25(9–11): 1293–1300.

Jeon, Y. C. et al. 2008. "Strain-Induced Martensitic Phase Transformation by Low-Cycle Fatigue in AISI 316L Stainless Steel." Materials Science Forum 580–582: 597–600.

Jinlong, Lv, Liang Tongxiang, and Wang Chen. 2016. "Surface Enriched Molybdenum Enhancing the Corrosion Resistance of 316L Stainless Steel." Materials Letters 171: 38–41.

Kumar, Chandra Shekhar, Kausik Chattopadhyay, Vakil Singh, and Girija Shankar Mahobia. 2020. "Enhancement of Low-Cycle Fatigue Life of High-Nitrogen Austenitic Stainless Steel at Low Strain Amplitude through Ultrasonic Shot Peening." Materials Today Communications 25(March): 101576.

Kundu, Amrita, and Pravash Chandra Chakraborti. 2010. "Effect of Strain Rate on Quasistatic Tensile Flow Behaviour of Solution Annealed 304 Austenitic Stainless Steel at Room Temperature." Journal of Materials Science 45(20): 5482–89.

Lei, Y. B., Z. B. Wang, J. L. Xu, and K. Lu. 2019. "Simultaneous Enhancement of Stress- and Strain-Controlled Fatigue Properties in 316L Stainless Steel with Gradient Nanostructure." Acta Materialia 168: 133–42.

Li, Xifeng et al. 2013. "Influence of Strain Rate on Tensile Characteristics of SUS304 Metastable Austenitic Stainless Steel." Acta Metallurgica Sinica (English Letters) 26(6): 657–62.

Lu, K., and J. Lu. 2004. "Nanostructured Surface Layer on Metallic Materials Induced by Surface Mechanical Attrition Treatment." Materials Science and Engineering A 375–377(1-2 SPEC. ISS.): 38–45.

Nishiguchi, Shigeru et al. 2001. "Proliferation and Differentiation Parameters of Human Ostleoblasts on Titanium and Steel Surfaces." Journal of Biomedical Materials Research 54(2): 209–15.

Pham, M. S., S. R. Holdsworth, K. G.F. Janssens, and E. Mazza. 2013. "Cyclic Deformation Response of AISI 316L at Room Temperature: Mechanical Behaviour, Microstructural Evolution, Physically-Based Evolutionary Constitutive Modelling." International Journal of Plasticity 47: 143–64.

Praveen, K V U, and Vakil Singh. 2008. "Effect of Heat Treatment on Coffin – Manson Relationship in LCF of Superalloy IN718." 485: 352–58.

Shen, Y. F. et al. 2012. "Twinning and Martensite in a 304 Austenitic Stainless Steel." Materials Science and Engineering A 552: 514–22.

Sivakumar, M., U. Kamachi Mudali, and S. Rajeswari. 1995. "Investigation of Failures in Stainless Steel Orthopaedic Implant Devices: Pit-Induced Fatigue Cracks." Journal of Materials Science Letters 14(2): 148–51.

Song, M. S., Y. Y. Kong, M. W. Ran, and Y. C. She. 2011. "Cyclic Stress-Strain Behavior and Low Cycle Fatigue Life of Cast A356 Alloys." International Journal of Fatigue 33(12): 1600–1607.

Tang, Yee Chin, Shoji Katsuma, Shinji Fujimoto, and Sachiko Hiromoto. 2006. "Electrochemical Study of Type 304 and 316L Stainless Steels in Simulated Body Fluids and Cell Cultures." Acta Biomaterialia 2(6): 709–15.

Verma, Preeti, N. C.Santhi Srinivas, S. R. Singh, and Vakil Singh. 2016. "Low Cycle Fatigue Behavior of Modified 9Cr-1Mo Steel at Room Temperature." Materials Science and Engineering A 652: 30–41.